applied sciences

MDPI

Article

Extraction of Impermeable Surfaces Based on Multi-Source Nighttime Light Images of Different Geomorphological Partitions

Jiashuo Zhang [1,2], Zhongfa Zhou [1,3,*] and Denghong Huang [1,3]

1 School of Karst Science, Guizhou Normal University, Guiyang 550001, China
2 The State Key Laboratory Incubation Base for Karst Mountain Ecology Environment of Guizhou Province, Guiyang 550001, China
3 State Engineering Technology Institute for Karst Desertification Control, Guiyang 550001, China
* Correspondence: fa6897@gznu.com

Abstract: Accurate extraction of impermeable surfaces is important for assessing land use change and improving the urban heat island effect. Nighttime light imagery has the advantage of being efficient and cost effective, providing a new perspective for monitoring and extracting impermeable surfaces and analyzing urban expansion processes. However, for the vast Karst terrain fragmentation area located in southwest China, the extraction of impermeable surface information faces many challenges due to surface landscape fragmentation and nighttime light image resolution. These challenges include light spillover, oversaturation and limited understanding of spatial links with surface types at fine scales. This study uses Luojia1-01, NPP-VIIRS, and Flint as remote sensing data sources to examine the applicability of nighttime light images in extracting impermeable surfaces from geomorphologically complex areas. The results show that Luojia1-01 data can provide finer spatial details and more accurate impermeable surface extraction results than NPP-VIIRS and Flint data. The relative error of extracted area in regions with large topographic relief is higher than that in regions with flat topographic cuttings. The extraction results of the three images are spatially similar; however, the overall accuracy is poor, and a single nighttime light image is not the best solution for obtaining impermeable surface information in large scale terrain fragmentation areas. However, the integrated application of multi-source light images is a trend for future regional research and development, and the best way to extract impermeable surfaces in complex terrain areas should be explored in conjunction with other remote sensing data sources in the future.

Keywords: Luojia1-01; NPP-VIIRS; flint; impermeable surface; karst mountains; geomorphologically complex area

check for updates

Citation: Zhang, J.; Zhou, Z.; Huang, D. Extraction of Impermeable Surfaces Based on Multi-Source Nighttime Light Images of Different Geomorphological Partitions. *Appl. Sci.* **2023**, *13*, 3006. https://doi.org/10.3390/app13053006

Academic Editors: Sungho Kim and Atsushi Mase

Received: 18 December 2022
Revised: 28 January 2023
Accepted: 21 February 2023
Published: 26 February 2023

1. Introduction

Impermeable surfaces are areas dominated by man-made surfaces [1], which mainly include urban impermeable surfaces and construction sites. Due to the urban sprawl occurring globally, more and more impervious surfaces are replacing the original permeable surfaces [2]. These impervious surfaces affect the evaporation and infiltration of surface water, alter the absorption and reflection of solar radiation [3], and directly affect the hydrological cycle, surface temperature, and environmental quality of cities [4]. Therefore, accurate quantification of the percentage of impervious surfaces is important for understanding the urbanization process, urban hydrothermal cycle, and environmental detection [5,6].

The traditional method of extracting impervious surfaces obtains information about impervious surfaces by manually identifying the relevant feature information of remote sensing graphics and distinguishing different features. This method faces many difficulties in its implementation in the underdeveloped areas due to the huge workload that requires a significant amount of labor effort and can easily cause errors. Furthermore, the extraction process is long, inefficient, and costly [7]. The rapid development of remote sensing theory and applications has shown its great potential to achieve understanding of various socioeconomic indicators related to human activities, providing a new approach to impermeable surface mapping [2]. Unlike traditional manual mapping carried out by governments or international organizations, remote sensing measurements are highly robust against human error. Moreover, they are very effective and can provide more objective results [8].

The selection of remote sensing data with suitable spectral, temporal, and spatial characteristics is the first important step in extracting impermeable surfaces using remote sensing. Previously, Landsat Thematic Mapper (TM) images were mostly applied for impermeable surface extraction [9]. Among these images, fine spatial resolution images contain richer spatial information (e.g., land use and land cover) and image features (buildings and roads), which facilitate the estimation and mapping of impervious surface extent [10]. Common methods for impervious surface extraction using the TM images include the normalized vegetation index (NDVI) [11], categorical regression tree (CART) algorithm [9], linear spectral mixture analysis (LSMA) medium-resolution extraction method [10], artificial neural networks [12], and impervious surface mapping based on high spatial resolution images. Landsat imagery can provide rich spectral, spatial, and temporal features. However, the spectral and spatial features are not sufficient for understanding the surface coverage type [13] from Landsat images. These images generally have a revisit period of 16 days, but reliable observations for a ground scene are obtained less frequently than 16 days because of interference from clouds and snow and their shadows. In addition, the Landsat 7 satellite has missing bands in the ETM+ data due to scan line failures. Unreliable observations caused by clouds, cloud shadows, snow and ice, and stripes limit the availability and mapping accuracy of multi-temporal Landsat images [14]. Therefore, it is difficult to obtain multi-year impermeable surface information at large spatial scales using the TM imagery.

With the advent of the Operational Line Scan System (OLS) of the Defense Meteorological Satellite Program (DMSP), nighttime lights were used in various applications. Elvidge et al. discovered a positive correlation between the degree of impermeability and light intensity, and demonstrated the applicability of nighttime light data in impermeable surface detection [15]. Unlike the sensors that detect surface objects based on the reflective properties of solar radiation, nighttime light images have the appropriate spatial and temporal resolution to detect large spaces of impermeable surfaces and the dynamic process of impermeable surface expansion [16]. At the same time, impervious surfaces are active areas of urban development, and the extraction of impervious surfaces from traditional remote sensing data is not effective for reflecting the social and economic activity of the region. On the other hand, the brightness of nighttime light data can accurately reflect the urban expansion level, and the intensity of lights can also reflect the scale of human activities within the city. Therefore, nighttime light data are more practical than the impervious surface extracted from traditional remote sensing images [17,18]. Consequently, nighttime light images have received a significant amount of attention as a new remote sensing data type [19].

There are five main types of available nighttime light images, which are described as follows:

The operational line system (OLS) sensor was launched in 1976 via the DMSP satellite. It is an oscillating scanning radiometer with a strip width of about 3000 km, consisting of two broad spectral bands [20]. It has a spatial resolution of 30 arc seconds [21]. As the DMSP-OLS nighttime light imagery is not perturbed by light shadows, it can be used for characterizing human activities, and is a good data source for dynamic monitoring of urban land expansion at large urbanization scales [22].

The Suomi national polar partnership (NPP) satellite launched in October 2011 has an on-board visible infrared imaging radiometer suite (VIIRS) instrument, which is a 22-band visible/infrared sensor. It has the same strip width as the DMSP, i.e., 3000 km, but a higher spatial resolution of 15 arc seconds [23]. The VIIRS has fuller in-flight calibration, lower detection limits, wider dynamic range, and finer radiometric quantification. Furthermore, it can provide richer information about human habitation and economic activity compared to the OLS [24].

As the first dedicated nighttime light satellite, Luojia1-01 has a spatial resolution of 130 m [25], a high radiance quantification of 15 bits, and a wide image frame of 250 km [26]. It provides a new nighttime light dataset with a high resolution and accuracy for artificial nighttime light variation monitoring [27]. It is seminal for the development and application of nocturnal remote sensing [28]. Since Luojia1-01 data do not suffer from saturation and bloom problems [29], Li et al. [30] found that the use of these data resulted in better impermeable surface extraction compared to using the NPP-VIIRS data.

The existing high-resolution nighttime light data are mainly photographs taken by astronauts on the international space station (ISS) and commercial satellites, such as EROS-B and JL1-3 [31]. The data obtained from the ISS have a spatial resolution between 5 to 200 m, while those obtained from the commercial satellites have a resolution of less than 1 m [32]. This category of data has the advantage of fine resolution and multISDectral information. However, their high price and difficult acquisition have lowered the interest in their usage for impermeable surface extraction and urban land expansion.

Derived datasets for nighttime lighting: Chen et al. produced a global "NPP-VIIRS-like" nighttime light dataset having a spatial resolution of 500 m with cross-sensor correction. These nighttime light data can effectively mitigate the oversaturation and overflow effects of the original DMSP-OLS data and use both types of data continuously over a time span [33]. Flint, developed by the Chinese Academy of Sciences Remote Sensing Satellite Ground Station, is the world's first full sequence global nighttime light annual product based on the NPP-VIIRS sensor's monthly nighttime light product. It has a 500 m resolution in its official version and a 1500 m resolution in its beta4 version. The Flint nighttime light images smooth out disturbances other than the surface factors and provide higher accuracy, stability, and ease of use to continuously track human activities on the Earth's surface [34]. However, the derived datasets have not been widely used in various fields.

Main existing methods for mapping impervious surfaces are as follows:

(1) Threshold segmentation methods that include: the ① Empirical threshold method, which is the extraction of urban areas by artificially setting specific thresholds based on the validation of previous studies [35]; ② Mutation detection method proposed by Imhoff et al. [36], which is based on the assumption that urban impervious surfaces consist of intact patches, and, by gradually increasing the segmentation nighttime lighting threshold, the obtained polygonal patches represent the urban areas along the edges. When the segmentation threshold reaches a point where a polygonal patch breaks up from within, the perimeter of the polygon representing the urban area suddenly increases. Pixels with values greater than or equal to this threshold are considered part of the impervious surface area.

(2) Data comparison methods that include: the ① Statistical Comparison Method, which uses the impervious surface area statistics released by the government as a reference and compares the difference between the extracted impervious surface area and the statistics. A threshold is generated iteratively until the extracted urban area matches the statistics [37]. ② Spatial comparison method, which uses high resolution multISDectral remote sensing data or land use data as auxiliary data to achieve urban impervious surface information extraction [38].

However, there are still several outstanding problems with the extraction of impermeable surfaces using nighttime light imagery. These problems are as follows:

(1) The scale and values of lights can become inconsistent with actual conditions due to cloud diffraction, moonlight, etc. [39]. This error may be amplified in topographically fragmented areas, and it becomes impossible to accurately represent the urban morphology of a region [40]. Consequently, there has been considerable discussion on

the utility of nighttime light imagery in topographically fragmented areas for truly representing the urban form of complex landscapes.

(2) Topographic conditions strongly influence the spatial distribution of nighttime lights and human activities. The spatial correlation between nighttime light images and surface types at fine scales [41] is essential for the application of nighttime light images for impermeable surface extraction. However, because of the late start of research on nighttime remote sensing data in China (a study of population change in important cities in mainland China based on nighttime light data), there are only a few studies on Karst mountains, and the existing empirical studies mainly analyze their relationships with various social environments. Meanwhile, in practical applications, "remote and inaccessible areas" are not perfectly distributed within a specific administrative area. From a geographical perspective, economic and social development emphasizes the process and state of achieving or failing to achieve coordinated development of "people", "industry", and "land" in a specific spatial and temporal context [42]. The socio-economic situation of any region has its own specific geographical background. The study of the application of nighttime light images should emphasize its usage in a regional context and not remain limited to a specific administrative area. It should provide the theory and applications that can be applied to different regions in similar natural environment backgrounds.

The Karst mountains of southwest China form a typically complex geomorphological region [43], which, together with the cloudy and rainy climatic characteristics, possibly renders the impervious surface extracted by night lighting spatially displaced. Therefore, it is of great significance to analyze the applicability of nighttime light image datasets in impermeable surface extraction in the southwest Karst mountains. This analysis is relevant vis-a-vis the application of nighttime light images in impermeable surface extraction for complex geomorphological regions and the in-depth mining of nighttime light image data. At the same time, topography and geomorphology are two key environmental factors governing human use and modification of land resources, which are deeply involved in the formation and change process of regional land use. Therefore, based on the geomorphological characteristics of the Karst mountains, this paper divides the study area into different geomorphological regions for analysis. Considering the complexity of the types of geomorphological areas in the Karst mountains and the data availability, three data sources are used:

(1) Luojia1-01 nighttime light data, which do not have saturation and blooming issues;
(2) NPP-VIIRS nighttime light data, which are the most widely used in current research; and
(3) "Flint" nighttime light data, which can smooth out disturbances other than surface factors.

This study analyzes the potential of different nighttime light image datasets for impermeable surface extraction in topographically fragmented areas. It contributes to the extension of the application potential of nighttime light imagery and supports subsequent research on mitigating urban climate change and reducing the impact of global warming on humans, which is important for the sustainable development of the region.

2. Materials and Methods

2.1. Overview of the Study Area

The Karst region in southwest China is centered on the Guizhou plateau. It is the largest and the most concentrated contiguous ecologically fragile mountainous area in the world. It has an area of more than 55×104 km^2, which is affected by the Karst environment, fragile ecological environment, and high occurrence possibility of natural disasters. Regional socio-economic development is heavily influenced by the landscape and faces many obstacles. Figure 1 shows that the geographical location of the Guizhou Province is 103°36′ E–109°35′ E, 24°37′ N–29°13′ N. Its topography ranges from high in the west to low in the east, sloping from the middle to the north, east, and south, with an altitude range of 130~2990 m and a large drop.

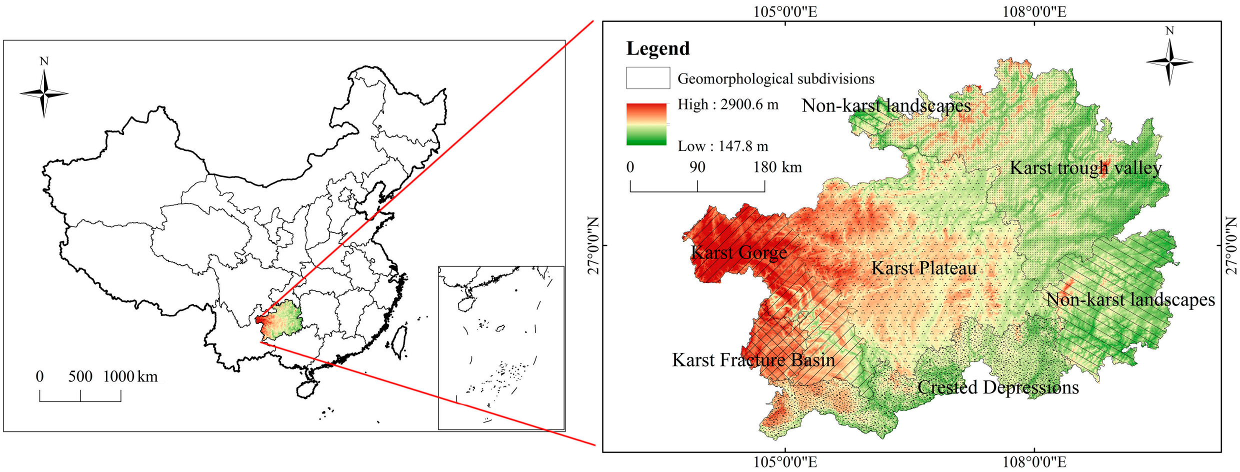

Figure 1. Geomorphological zoning map of the study area.

2.2. Data Preprocessing

2.2.1. Luojia1-01

The Luojia1-01 nighttime lighting product used in this paper is a data product downloaded from the geospatial data cloud (http://www.gscloud.cn/) accessed on 1 August 2018). It has a resolution of 130 m and contains a high amount of noise. Therefore, first, the data are denoised using a filter in ArcGIS. The effect of light saturation is mitigated by using the Luojia1-01 data provided by the data distribution website for radiation correction [44], as follows:

$$DN_i = DN^{\frac{3}{2}} \times 10^{-10} \tag{1}$$

where DN is a number indicating the image value of each pixel, and DN_i denotes the image element value after radiometric correction. The original Luojia1-01 radiance units given in W-m-2-Sr-1 μm-1 are converted to nanometers as W-cm-2-Sr-1 in order to facilitate comparison of data from multiple sources.

2.2.2. NPP-VIIRS

The NPP-VIIRS nighttime lighting product is available on the national oceanic and atmospheric administration's website (https://www.ngdc.noaa.gov/eog/viirs) accessed on 1 August 2018. It is a monthly composite nighttime light product with a resolution of 500 m. The negative values in the downloaded NPP-VIIRS images are first eliminated, and, subsequently, the data are corrected for relative radiation as described in [45].

2.2.3. Flint

Flint nighttime light data are the world's first full range of Global High Definition (HD) nighttime light products that are built on the NPP-VIIRS sensor's monthly nighttime light products. Compared to the original product, the Flint nightlight data offer greater accuracy, stability, ease of use, and the ability to describe the distribution of nighttime light brightness and darkness. In addition, these data describe changes over a five-year period, which can be used to continuously track human activity on the Earth's surface. The Flint nightlight dataset is downloaded from http://satsee.radi.ac.cn/cfimage/nightlight/ accessed on 1 August 2018. The dataset belongs to the beta4 version product with a resolution of 1500 m. These data correspond to products that have already been processed and, therefore, they were not pre-processed.

2.2.4. Unified Scale

Thirty uniformly distributed ground control points were manually collected from the study area boundaries. The three nighttime light images were geometrically corrected using the Landsat 8 imagery with a uniform spatial coordinate system of WGS1984. The three corrected Luojia1-01, NPP-VIIRS, and Flint datasets were cropped using ArcGIS 10.2. The images were projected in the Lambert equal area projection coordinate system and resampled to achieve identical resolutions of 100 m. Figure 2 shows the corrected images separately. Areas with monthly mean NDVI > 0.9 and NDVI < 0.1 are excluded as uninhabited areas [43,44].

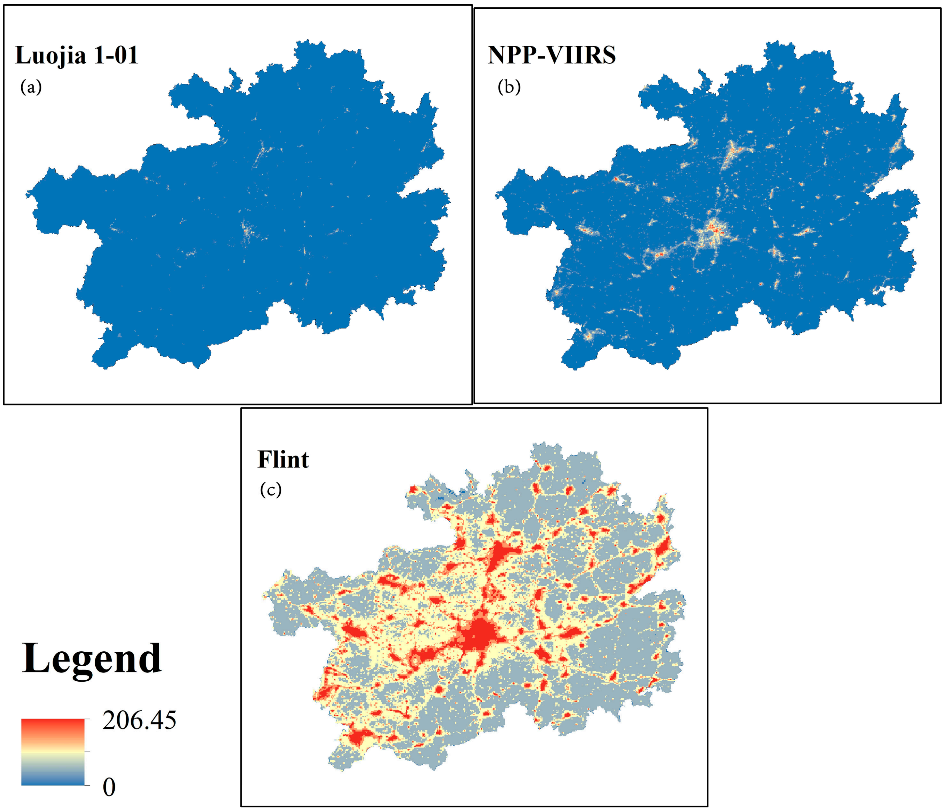

Figure 2. Corrected nighttime light images: (**a**) Luojia1-01 corrected image; (**b**) NPP-VIIRS corrected image; (**c**) Flint corrected image.

2.2.5. Other Data

The impervious surface data were obtained from [46]. Reference to data on the classification of landform types exists in [44].

2.3. Research Methodology

2.3.1. Impermeable Surface Extraction

Unlike regions with flat topography, the Karst mountains have a broken topography. Furthermore, the distribution of impermeable surfaces is affected by rugged topography, land resources, transportation, ethnic culture, and other factors. The spatial distribution pattern of impermeable surfaces varies significantly [47] and, consequently, large errors can occur if the impermeable surfaces are extracted according to a uniform standard. Therefore, prior to the extraction, the study area is first classified according to the type of landform: Karst fault basins, Karst gorges, Karst plateaus, Karst troughs, crested depressions, and non-Karst landforms.

The implementation of the mutation detection method [42] relies only on the features present in the nighttime lighting data itself and exhibits a minor dependence on other conditions, e.g., built-up area, actual built-up area image data, etc. At the same time, the extraction results are more accurate compared to the empirical threshold method. Therefore, this study uses the mutation detection method to extract impermeable surfaces from the Karst topographically fragmented areas. The specific steps of the extraction method are as follows:

(1) The ROI module of ENVI is used to extract queue values for light segmentation.
(2) The polygonal patches representing the urban areas are gradually reduced along the edges while the segmentation nighttime light threshold is gradually increased.
(3) When the segmentation threshold reaches a certain point, the polygon patch breaks up from inside and its perimeter representing the urban area suddenly increases. This is the threshold point for extracting the impermeable surface area. The pixels whose values are greater than or equal to the threshold are considered as part of the impermeable surface area.

2.3.2. Accuracy Verification

In this paper, the impermeable surfaces are extracted in the form of an image. The extraction accuracy is verified by calculating the coefficient of determination (R^2), root mean square error (*RMSE*), and systematic error (*SE*) [48] for 200 sample points of images per region. The R^2 and *SE* can be used to measure the systematic error and the goodness of fit of the simulated impervious surface coverage values with respect to the true coverage values, respectively. The *RMSE* is highly sensitive to very large or small errors in a set of measurements, and can effectively reflect the precision of the measurements [49]. The expressions for calculating R^2, *RMSE* and *SE* are as follows:

$$R^2 = 1 - \frac{\sum_{i=1}^{N} (x_1 - x_i)^2}{\sum_{i=1}^{N} (x_1 - x_2)^2}$$

$$RMSE = \sqrt{\frac{\sum_{i=1}^{N} (x_i - x_1)^2}{N}}$$

$$SE = \frac{\sum_{i=1}^{N} (x - x_i)}{N}$$

where x is the impervious surface estimate, x_1 is the true impervious surface value, x_2 is the mean of the true impervious surface value, and N is the sample size. The smaller the values of *RMSE* and *SE*, the smaller the impervious surface estimation error. Values of $SE > 0$ and $SE < 0$ mean that the impervious surface is overestimated and underestimated, respectively.

The error in extracting the impervious surface area is obtained as follows:

$$relative\ error = \frac{x_i - x}{x}$$

where x and x_1 are the estimated and true impervious surface areas, respectively.

3. Results

3.1. Impermeable Surface Extraction

3.1.1. Impervious Surface Extraction Results

Figure 3 shows the variation in extraction queues and the corresponding impervious surface patch perimeters for each dataset under different geomorphological partitions. The curves in the figure demonstrate that the polygon perimeter of the urban area gradually decreases as the segmentation threshold increases gradually. When the threshold increases to a certain queue value, the polygon perimeter starts to increase and then decreases gradually. This queue value is the optimal threshold point for extracting the impervious surface of the city.

Figure 4 shows the impermeable surfaces extracted from six different geomorphological divisions in the Karst Mountains based on Luojia1-01, NPP-VIIRS, and Flint nighttime light images, using the queues shown in Figure 3. The extracted surfaces are compared with the real impermeable surfaces. Overall, the results extracted using the three nighttime light images exhibit similar spatial patterns.

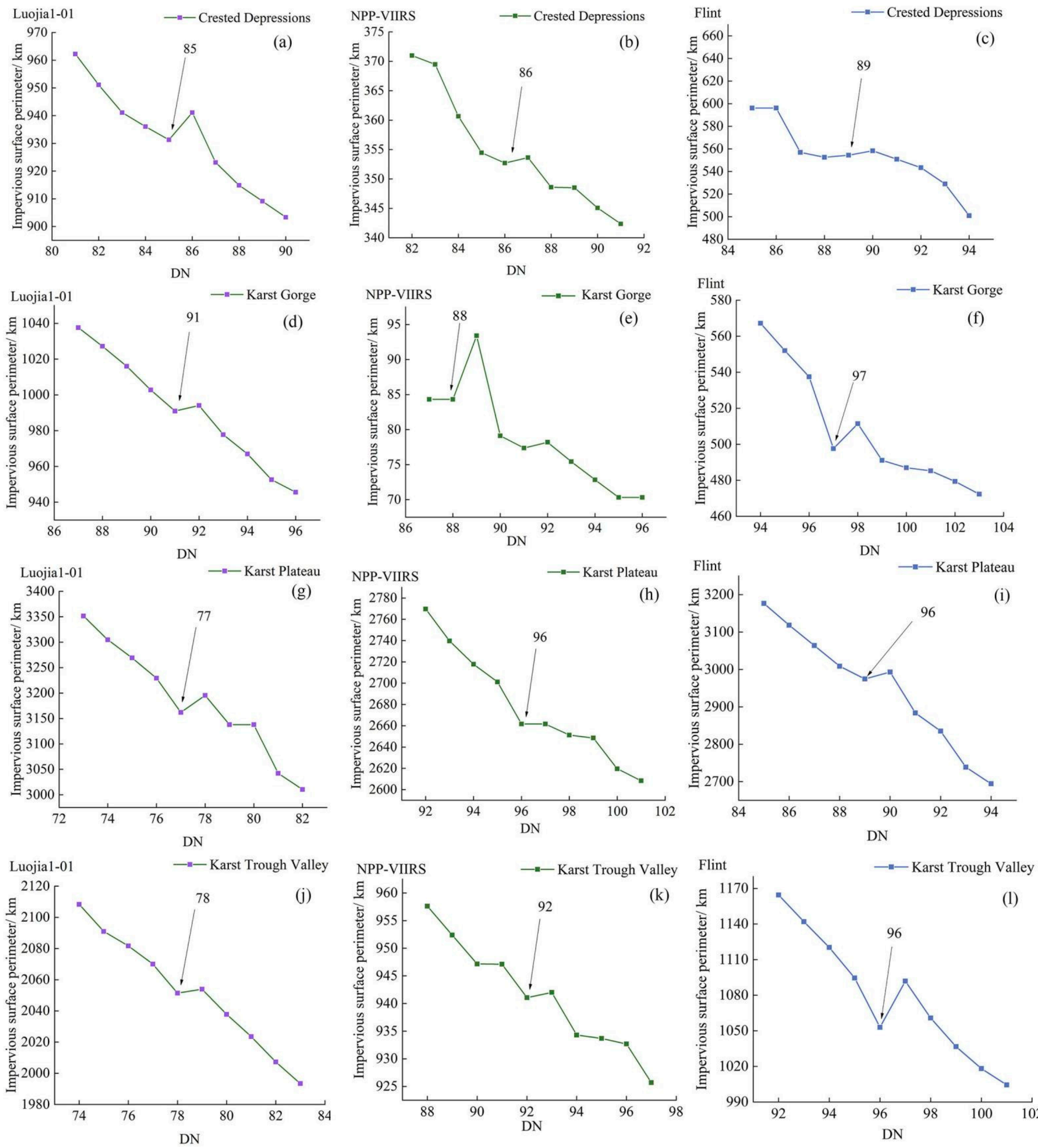

Figure 3. *Cont.*

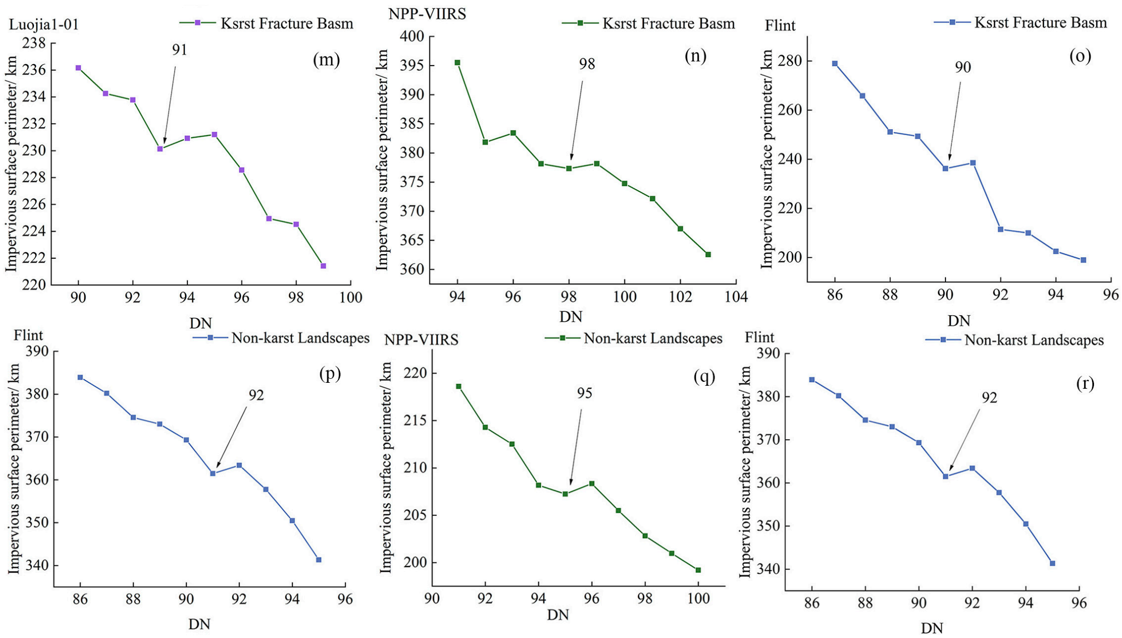

Figure 3. Variation in perimeter of built-up area patches extracted based on different queue values: (**a**) variation of perimeter of Crested Depressions built-up area patches extracted from Luojia1-01 with different queue values; (**b**) variation of perimeter of Crested Depressions built-up area patches extracted from NPP-VIIRS with different queue values; (**c**) variation of perimeter of Crested Depressions built-up area patches extracted from Flint with different queue values; (**d**) variation of perimeter of Karst Gorge built-up area patches extracted from Luojia1-01 with different queue values; (**e**) variation of perimeter of Karst Gorge built-up area patches extracted from NPP-VIIRS with different queue values; (**f**) variation of perimeter of Karst Gorge built-up area patches extracted from Flint with different queue values; (**g**) variation of perimeter of Karst Plateau built-up area patches extracted from Luojia1-01 with different queue values; (**h**) variation of perimeter of Karst Plateau built-up area patches extracted from NPP-VIIRS with different queue values; (**i**) variation of perimeter of Karst Plateau built-up area patches extracted from Flint with different queue values; (**j**) variation of perimeter of Karst Trough Valley built-up area patches extracted from Luojia1-01 with different queue values; (**k**) variation of perimeter of Karst Trough Valley built-up area patches extracted from NPP-VIIRS with different queue values; (**l**) variation of perimeter of Karst Trough Valley built-up area patches extracted from Flint with different queue values; (**m**) variation of perimeter of Karst Fracture Basm built-up area patches extracted from Luojia1-01 with different queue values; (**n**) variation of perimeter of Karst Fracture Basm built-up area patches extracted from NPP-VIIRS with different queue values; (**o**) variation of perimeter of Karst Fracture Basm built-up area patches extracted from Flint with different queue values; (**p**) variation of perimeter of Non-karst Landscapes built-up area patches extracted from Luojia1-01 with different queue values; (**q**) variation of perimeter of Non-karst Landscapes built-up area patches extracted from NPP-VIIRS with different queue values; (**r**) variation of perimeter of Non-karst Landscapes built-up area patches extracted from Flint with different queue values.

A comparison of the impermeable surfaces extracted from different data sources shows that the impermeable surfaces extracted from Luojia1-01 for the landform types other than the Karst fracture basins overlap more closely with the actual impermeable surfaces. The NPP-VIIRS images have higher spatial similarity to the Flint images. However, the impermeable surface patches extracted from the former type of images are highly separated. Furthermore, the extracted impermeable surface shows a poor spatial overlap with respect to the actual impermeable surface. The processed Flint dataset can effectively complement the detailed and missing information within the nighttime lighting data. Consequently, the impervious surface patches extracted from the Flint data are complete and highly aggregated but have blurred boundaries.

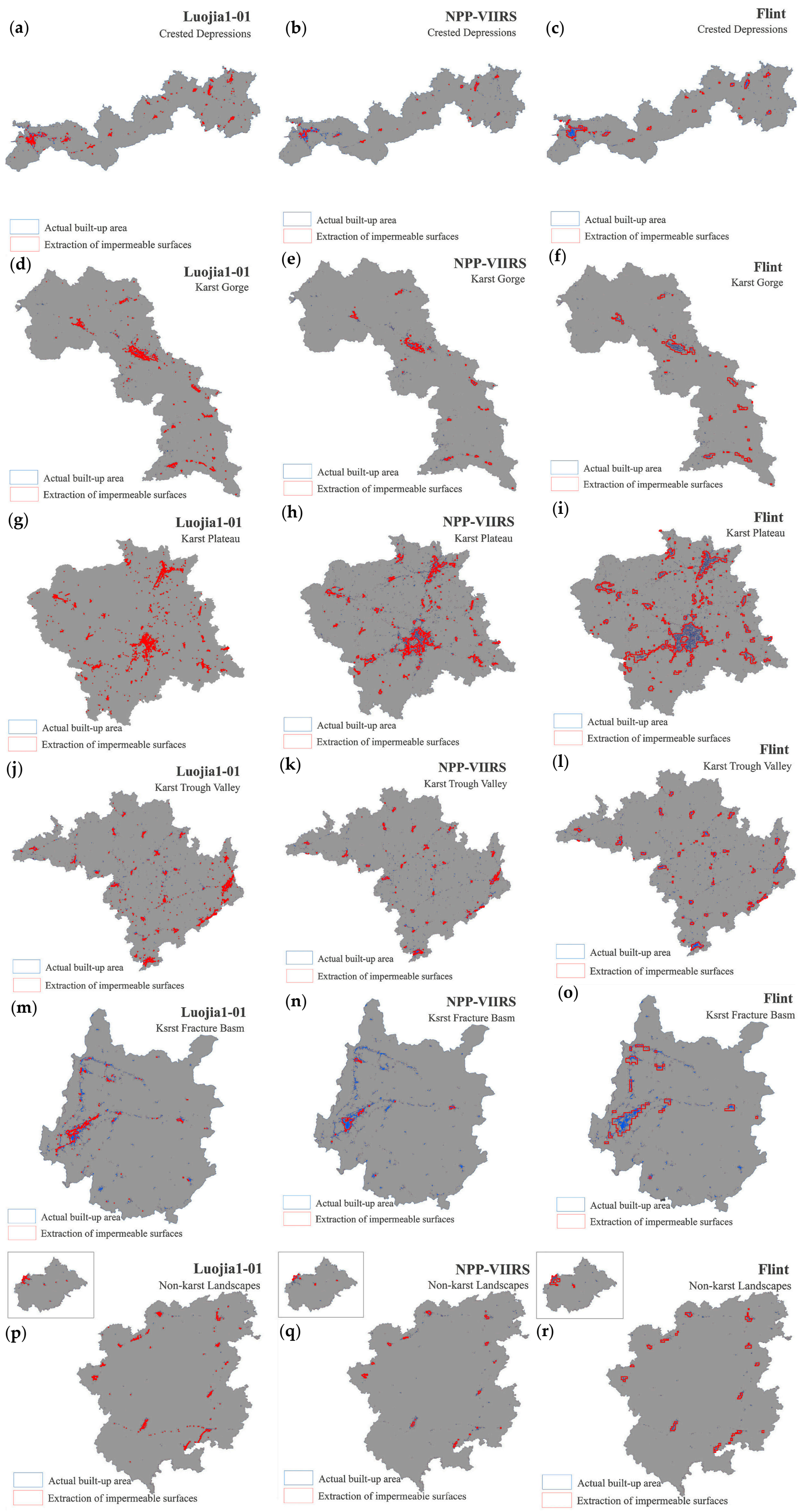

Figure 4. Ratio between the impervious surface extracted from different nighttime lighting data and the actual impervious surface. (**a**) Impervious surface and actual impervious surface of the Crested Depressions extracted from Luojia1-01; (**b**) Impervious surface and actual impervious surface of the Crested Depressions extracted from NPP-VIIRS; (**c**) Impervious surface and actual impervious surface

surface of the Crested Depressions extracted from Flint; (**d**) Impervious surface and actual impervious surface of the Karst Gorge extracted from Luojia1-01; (**e**) Impervious surface and actual impervious surface of the Karst Gorge extracted from NPP-VIIRS; (**f**) Impervious surface and actual impervious surface of the Karst Gorge extracted from Flint; (**g**) Impervious surface and actual impervious surface of the Karst Plateau extracted from Luojia1-01; (**h**) Impervious surface and actual impervious surface of the Karst Plateau extracted from NPP-VIIRS; (**i**) Impervious surface and actual impervious surface of the Karst Plateau extracted from Flint;(**j**) Impervious surface and actual impervious surface of the Karst Trough Valley extracted from Luojia1-01; (**k**) Impervious surface and actual impervious surface of the Karst Trough Valley extracted from NPP-VIIRS; (**l**) Impervious surface and actual impervious surface of the Karst Trough Valley extracted from Flint; (**m**) Impervious surface and actual impervious surface of the Karst Fracture Basm extracted from Luojia1-01; (**n**) Impervious surface and actual impervious surface of the Karst Fracture Basm extracted from NPP-VIIRS; (**o**) Impervious surface and actual impervious surface of the Karst Fracture Basm extracted from Flint; (**p**) Impervious surface and actual impervious surface of the Non-karst Landscapes extracted from Luojia1-01; (**q**) Impervious surface and actual impervious surface of the Non-karst Landscapes extracted from NPP-VIIRS; (**r**) Impervious surface and actual impervious surface of the Non-karst Landscapes extracted from Flint.

3.1.2. Impermeable Surface Density Extraction Results

Next, the impervious surface extraction accuracy at different Impervious Surface Density (ISD) values for the three nighttime lighting data are compared. This is carried out by classifying the extraction results for cities with different geomorphological types in the study area into five categories based on the ISD values: $0 \leq$ ISD < 0.2 (low density), $0.2 \leq$ ISD < 0.4 (low to medium density), $0.4 \leq$ ISD < 0.6 (medium density), $0.6 \leq$ ISD < 0.8 (medium to high density), and $0.8 \leq$ ISD ≤ 1 (high density). Figure 5 shows the results of the impervious surface density distribution obtained from the three data types. It can be observed that the results tend to be consistent in terms of the spatial distribution of the high-density impervious surface distribution. Furthermore, all the results form a high-density impervious surface concentration area centered on the central city. The high-density impervious surface area extracted from the Flint data in Karst gorge and crested depressions is significantly higher than that extracted from the NPP-VIIRS and Luojia1-01 data. Meanwhile, the impervious surface density extracted from the NPP-VIIRS and Flint data in this area is significantly higher than that extracted from the Luojia1-01 data. The impervious surface density obtained from the Luojia1-01 data in the crested depressions and Karst plateau is considerably lower than that obtained from the NPP-VIIRS and Flint data. The impervious surface densities extracted from the Karst trough valley and non-Karst landscapes nighttime light data are similar, indicating that the impervious surface densities in flat and contiguous terrain are less affected by the resolution.

3.2. Impermeable Surface Accuracy Verification

3.2.1. Spatial Accuracy of Impervious Surfaces

Based on the impervious surface results obtained from the Luojia1-01, NPP-VIIRS, and Flint data, a total of 150 verification samples were randomly selected in each of the aforementioned six different geomorphological zones. These samples were compared with the actual impervious surface vector data. The impervious surface within each sample was vectorized using ArcGIS to obtain the true scale of each impervious surface and compared with the impervious surface results extracted from the three types of nighttime lighting image data. Figure 6 compares the spatial accuracy of the impervious surfaces obtained from the Luojia1-01, NPP-VIIRS, and Flint data. Overall, the impervious surface extraction accuracy was poor for all three data types. In addition, the use of a single nighttime light data source was not suitable for obtaining impervious surface information in large scale topographically fragmented areas. For the Karst plateau, impervious surfaces were extracted with the highest accuracy from the VIIRS/DNB data, while the urban impervious surfaces were extracted with a considerably higher accuracy from the Luojia1-01 data than the NPP-VIIRS and Flint data for the remaining five landscape types. This high accuracy is indicated by high R^2 values and low RMSE and SE values.

Figure 5. Density distribution of impervious surfaces extracted from different nighttime lighting data sources.

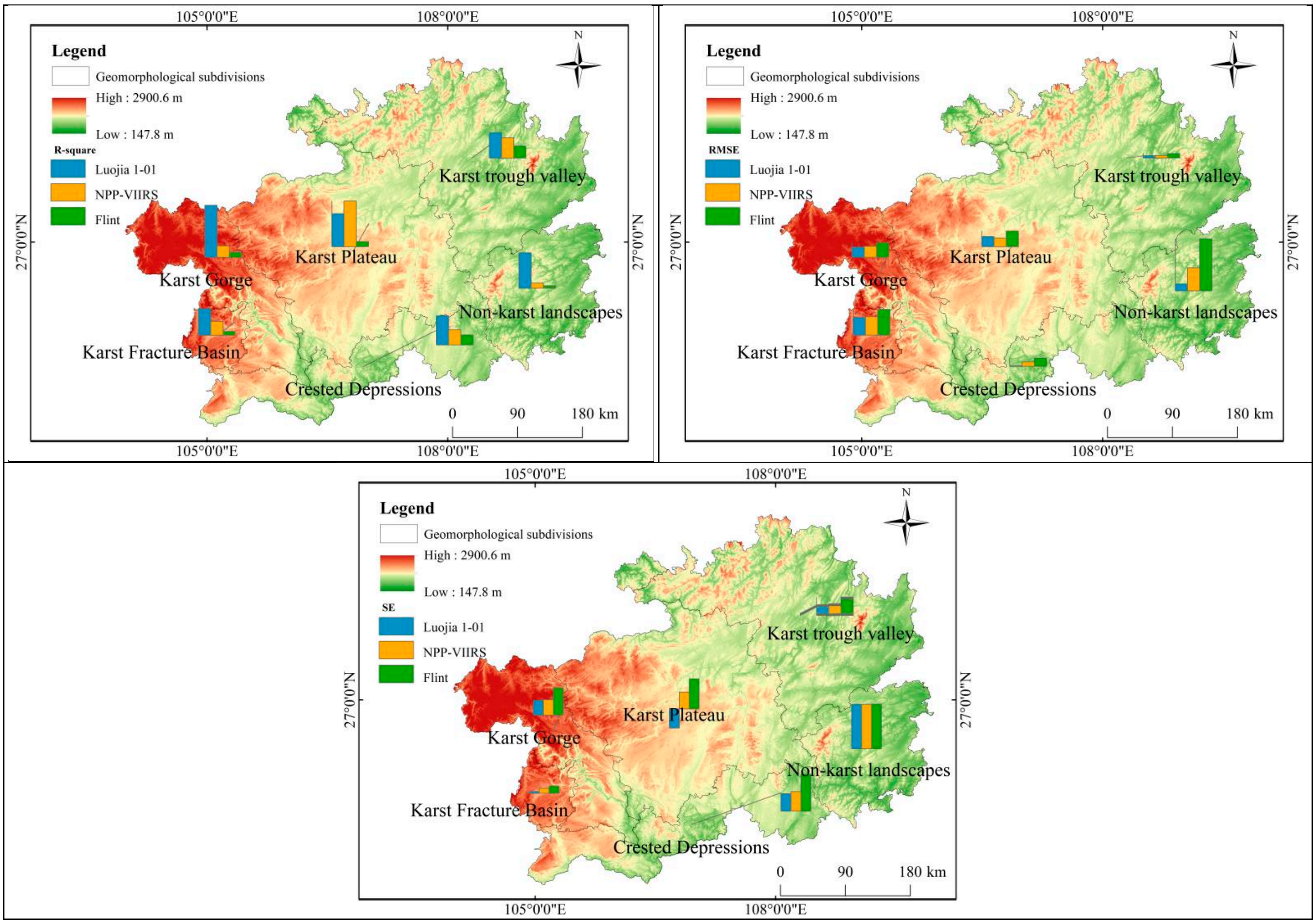

	Luojia1-01			NPP-VIIR			Flint		
	R2	RMSE	SE	R2	RMSE	SE	R2	RMSE	SE
Crested Depressions	0.23	0.02	0.58	0.12	0.17	0.65	0.08	0.31	1.22
Karst Gorge	0.41	0.39	0.49	0.09	0.42	0.51	0.04	0.56	0.91
Karst Plateau	0.26	0.38	−0.63	0.36	0.33	0.56	0.04	0.59	1.00
Karst Trough Valley	0.20	0.09	−0.02	0.16	0.10	−0.05	0.10	0.17	−1.35
Karst Fracture Basin	0.21	0.68	0.06	0.11	0.7	0.16	0.03	0.98	0.24
Non-Karst Land-scapes	0.28	0.26	1.47	0.04	0.87	1.47	0.02	1.97	1.47

Figure 6. Comparison results of spatial accuracy of impermeable surfaces.

The above results suggest that the Luojia1-01 data are more suitable for extracting impervious surfaces in topographically fragmented areas than the NPP-VIIRS and Flint data. The SEs of all three data sources are greater than zero for all landscape types, except for the impervious surface extracted from the Luojia1-01 data in Karst plateau. This indicates that the use of Luojia1-01 data causes underestimation in the Karst plateau and overestimation in the rest of the density range, while the use of both NPP-VIIRS and Flint data leads to overestimation in all landscape types. This phenomenon is mainly caused by the low resolution of the NPP-VIIRS and Flint data and the outward spillover of the data itself, which results in overestimation of the impervious surface.

3.2.2. Impervious Surface Area Error

Figure 7 shows the relative error between the extracted and actual impervious surfaces for different landform types. Statistically, the impervious surface area extracted from the Luojia1-01 nighttime light image is more accurate than the actual impervious surface area.

Furthermore, the impervious surface extracted using the NPP/VIIRS nighttime light image does not contain any information about the rest of the landform types, except for the Karst fracture basin. The impervious surface extracted using the Flint nighttime light images is the least accurate as it is significantly larger than the actual impervious surface area.

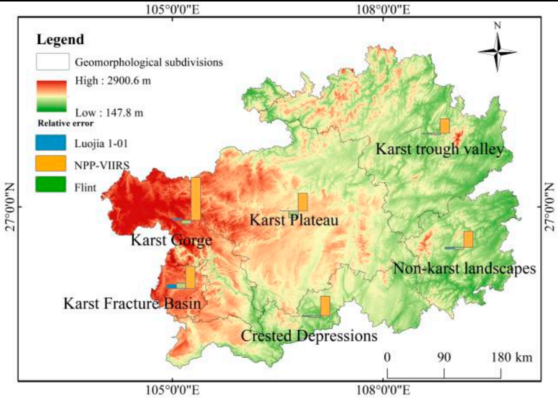

	Luojia1-01	NPP-VIIRS	Flint
Crested Depressions	−8.67%	−16.31%	211.24%
Karst Gorge	18.21%	-38.43%	458.88%
Karst Plateau	0.70%	−74.38%	187.84%
Karst Trough Valley	−3.94%	−17.55%	154.00%
Karst Fracture Basin	42.21%	56.37%	240.26%
Non-karst Landscapes	−16.41%	−24.76%	171.89%

Figure 7. Average relative error of urban impervious surface extraction results for different landform types.

It can be gathered from the results of the different landform types that the errors in the extraction of the impermeable surfaces using the three nighttime light images in the Karst gorge and Karst fracture basin landform types are higher than those in the other flat and contiguous areas. This indicates that the topography influences the application of nighttime lighting, with the error in extracting impervious surface area in broken topography regions being significantly higher than that in flat and contiguous topography regions. The use of NPP-VIIRS images results in a lower impervious surface area error for the Crested Depressions (error = −16.31%) and Karst Trough Valley (error = −17.55%). The use of Flint images resulted in the least errors for impervious surface area extraction for Karst Trough Valley (error = 154.00%), Non-Karst Landscapes (error = 171.89%) and Karst Plateau (error = 187.84%). This indicates that the Luojia1-01 data provide a greater advantage in extracting impervious surface in economically developed, light-concentrated, and contiguous areas, while the NPP-VIIRS and Flint images are more influenced by topography than the Luojia1-01 images for impervious surface extraction.

4. Discussion and Conclusions

4.1. Discussion

4.1.1. Accuracy Analysis

Overall, the Luojia1-01 data provided finer spatial details and more accurate impervious surface extraction results due to spatial resolution. The extraction results obtained with the three nighttime light images showed similar spatial patterns: (1) The impervious surface of the remaining landform types extracted using the Luojia1-01 data exhibited a higher degree of overlap with the actual impervious surface. (2) The impervious surface patches extracted using the NPP-VIIRS showed a high degree of separation. (3) The extraction of impervious surface patches using the Flint data demonstrated a complete and high degree of aggregation. However, the extracted impervious surfaces contained blurred boundaries. The results of the extraction of impervious surface densities in the flat topography and economically developed areas were less sensitive to image resolution.

In terms of the spatial accuracy of the extraction results, the Luojia1-01 data were more accurate than the NPP-VIIRS and Flint data. However, the accuracy of impervious surface extraction was poor with all three data types. Furthermore, the extraction of impervious surfaces using only nighttime light data was not effective for obtaining impervious surface information in areas with large scale topographic fragmentation. The results with the Luojia1-01 data were underestimated in the Karst plateau and overestimated in the rest of the density range, while the results with both NPP-VIIRS and Flint data were overestimated in all landscape types. This behavior was mainly caused by the low resolution of the NPP-VIIRS and Flint data, and the overestimation of impervious surface due to the overflow of values from the data itself.

4.1.2. Error Analysis and Insights

In terms of the relative error of the extracted area, the error in the application of nighttime lighting was significantly higher in areas with broken terrain than in areas with flat and contiguous terrain. In addition, the errors in the extraction of impervious surface area statistics were considerably higher in the Karst gorge, Karst plateau, and Karst fracture basin landform types than in other areas with a flat terrain. The Luojia1-01 data provided a greater advantage in extracting impervious surface from economically developed and light concentrated areas, while the extraction of impervious surfaces from the NPP-VIIRS and Flint data was influenced more by topography than the Luojia1-01 data.

The results showed that the application of nighttime light images to impervious surfaces was affected by topography, and the impervious surface extraction had poor accuracy. The single use of nighttime light data to extract impervious surfaces was not effective for obtaining impervious surface information in large scale topographic fragmentation areas. At the same time, the extraction of impermeable surfaces in cities with a fragmented topography and a small economic scale showed that the extraction accuracies of different nighttime light images were significantly different. The reasons for this phenomenon may include the following:

(i) Climatic conditions in the Karst mountains themselves. The cloudy and rainy climatic characteristics of the Karst mountains can easily bias the collected light data due to factors such as cloud cover, pollutants, and other light sources [44].
(ii) Zone modelling approach. There are complex reasons that affect the construction of impermeable surfaces in reality, including topography, social, economic and ecological aspects, etc. More complex factors should be considered in actual modelling, and using only geomorphology as the standard zoning approach may not be suitable for different types of nighttime light data.

Therefore, the integration of nighttime light image data with a variety of remote sensing data should be studied in detail in the future. This study can develop a highly accurate nighttime light image dataset, as well as investigate the interaction between various natural, social, and economic elements [45]. At the same time, it is necessary in the next stage of research to combine other remote sensing data sources, such as stone desertification data, NDVI, etc., to explore the best way for extracting impermeable surfaces in topographic fragmentation areas. Alternatively, other zoning methods can be used to analyze the nighttime light data of the topographic fragmentation areas in combination with different remote sensing data sources to accurately extract impermeable surfaces. The aforementioned steps are crucial to the monitoring of urban morphological changes.

Generally speaking, nighttime lights vary considerably over the course of a year and require data from at least a year or multiple years for comparison. However, the number of available data periods is small due to the short launch time of Luojia1-01. At the same time, due to the cloudy and rainy conditions in the Karst mountains, the only image with a minimum number of clouds among the available data periods is the one used in this paper. Therefore, additional multi-period data sources are needed in the future study to confirm the reliability of the conclusions presented in this paper.

4.1.3. Comparison with Existing Studies

In this study, impervious surfaces corresponding to different landform types in topographic fragmentation areas were extracted, and the results of the study contributed to the nighttime light images. First, the extraction queues of the three data showed that the accuracy of the three images in extracting the spatial extent of impervious area initially increased and then decreased with the increase in DN threshold value. The highest extraction accuracy based on Luojia1-01 also appeared in the larger range of DN values. This indicated that the Luojia1-01 data could provide finer spatial details compared to other data sources, which was consistent with the results of a previous study [50].

Second, comparing the extraction results obtained using Luojia1-01, NPP-VIIRS, and Flint nighttime lighting data demonstrated that the impermeable surfaces of three different types of cities extracted using the Flint data in topographic fragmentation areas showed the smallest error. However, the high spatial resolution of the Luojia1-01 image rendered it more sensitive to environmental changes compared with the lower resolution NPP-VIIRS and Flint images. Consequently, the impervious surface extraction from the Luojia1-01 data in topographically flat areas showed more errors in terms of omission and biased extraction results. On the other hand, the area of impervious surface extracted in topographically broken areas was larger than the actual impervious surface area. However, remote urban cores could be identified better using the Luojia1-01 data. In contrast, the impermeable surface extracted using the NPP-VIIRS data was more complete, which was consistent with the findings presented in [45].

Third, unlike the findings of previous studies, nighttime light imagery of topographically fragmented areas was less affected by light spillover and oversaturation effects, possibly due to cloudy conditions, monitoring time, etc. The only exception to this behavior was exhibited by Flint images. This behavior was inconsistent with our initial hypothesis that the spillover effects would be severe for nighttime light imagery of topographically fragmented areas. In previous studies that compared the application of different nighttime light imagery data sources, a few experts considered the Flint nighttime light data that could smooth out surface factors. However, in this study the impermeable surface extracted from the Flint nighttime light data was heavily influenced by over-saturation and had poor accuracy. This dataset needs to be further explored in subsequent studies to explore its potential applications.

Fourth, this study found that the impervious surface density extracted at different resolutions in the topographically flat and contiguous area was less affected by the resolution. At the same time, the extraction results from the three datasets tended to be consistent in spatial distribution in terms of high-density impervious surface distribution and formed a high-density impervious surface aggregation area centered on the central city. This is an area that has not been considered in previous studies, and the correlation between impervious surface density and topography should be analyzed further to provide theoretical support for the application of nighttime lighting.

Fifth, the mutation detection method used in this study extracts impermeable surfaces. In the process of extracting impermeable surfaces of Karst canyons using NPP-VIIRS data, the queue value 88 was selected as the queue point; however, a small increase in perimeter occurred after DN = 91. We reviewed the relevant literature and did not find any explanation for this phenomenon. We hypothesize that the specific reason may be due to the fragmentation of Karst canyon topography, which causes two peaks in the extraction process. This may be a novel finding in this paper, and a more detailed analysis of this finding is needed in subsequent studies.

4.2. Conclusions

The analysis of the applicability of nighttime light image datasets in the extraction of impermeable surfaces in the southwest Karst mountains is of great importance for their use in topographically fragmented areas and the in-depth mining of nighttime light image data. This study used Luojia1-01 nighttime light data, NPP-VIIRS nighttime light data, and Flint-derived nighttime light data to divide the study area into different geomorphological regions for analysis. It further investigated the potential of different nighttime light image datasets for impermeable surface extraction in terrain fragmentation areas. This work can contribute to the subsequent extension of the application potential of nighttime light imagery, supports research to reduce the impact of global warming on humans, and is important for achieving sustainable development of the region.

Author Contributions: Data curation, J.Z.; writing—original draft preparation, J.Z.; writing—review and editing, Z.Z. and D.H.; supervision, Z.Z.; project administration, Z.Z.; funding acquisition, Z.Z. All authors have read and agreed to the published version of the manuscript.

Funding: This research was funded by the National Natural Science Foundation of China Regional Projects, grant number 41661088, and the Guizhou Province "High-level Innovative Talents Training Program '100' Level Talents" Project, grant number (2016)5674.

Institutional Review Board Statement: Not applicable.

Informed Consent Statement: Not applicable.

Data Availability Statement: Not applicable.

Conflicts of Interest: The authors declare no conflict of interest.

References

1. Chowdhury, P.K.R.; Maithani, S. Monitoring growth of built-up areas in indo-gangetic plain using multi-sensor remote sensing data. *J. Indian Soc. Remote Sens.* **2010**, *38*, 291–300. [CrossRef]
2. Chen, Y.B.; Zheng, Z.H.; Wu, C.F.; Qian, Q.L. A review and outlook on the application of remote sensing data for nighttime lighting. *Adv. Geosci.* **2019**, *2*, 205–223.
3. Wang, Y.; Li, M. Urban Impervious Surface Detection from Remote Sensing Images: A review of the methods and challenges. *IEEE Geosci. Remote Sens. Mag.* **2019**, *7*, 64–93. [CrossRef]
4. Yu, Y.; Li, J.; Zhu, C.; Plaza, A. Urban Impervious Surface Estimation from Remote Sensing and Social Data. *Photogramm. Eng. Remote Sens.* **2018**, *84*, 771–780. [CrossRef]
5. Wang, H.; Lu, S.; Wu, B.; Li, X. Advances in remote sensing extraction of impermeable surfaces and applications. *Adv. Earth Sci.* **2013**, *3*, 327–336.
6. Zhang, T.; Huang, X. Monitoring of urban impervious surfaces using time series of high-resolution remote sens-ing images in rapidly urbanized areas: A case study of Shenzhen. *IEEE J. Sel. Top. Appl. Earth Obs. Remote Sens.* **2018**, *11*, 2692–2708. [CrossRef]
7. Wu, H. Quantitative Analysis of the Effect of Impervious Surface Coverage on Surface Temperature. Master's Thesis, Xiangtan University, Xiangtan, China, 2021. Available online: https://kns.cnki.net/KCMS/detail/detail.aspx?dbname=CMFD202201&filename=1022451492.nh (accessed on 1 June 2021).
8. Zhao, M.; Zhou, Y.; Li, X.; Cao, W.; He, C.; Yu, B.; Elvidge, C.D.; Cheng, W. Applications of Satellite Remote Sensing of Nighttime Light Observations: Advances, Challenges, and Perspectives. *Remote Sens.* **2019**, *11*, 1971. [CrossRef]
9. Goodchild, M.F.; Quattrochi, D.A. *Scale in Remote Sensing and GIS*; Lewis Publishers: New York, NY, USA, 2023.
10. Weng, Q. Remote sensing of impervious surfaces in the urban areas: Requirements, methods, and trends. *Remote Sens. Environ.* **2012**, *117*, 34–49. [CrossRef]
11. Yuan, F.; Bauer, M.E. Comparison of impervious surface area and normalized difference vegetation index as indicators of surface urban heat island effects in Landsat imagery. *Remote Sens. Environ.* **2007**, *106*, 375–386. [CrossRef]
12. Yang, L.; Huang, C.; Homer, C.G.; Wylie, B.K.; Coan, M.J. An approach for mapping large-scale impervious sur-faces: Synergistic use of Landsat-7 ETM+ and high spatial resolution imagery. *Can. J. Remote Sens.* **2003**, *29*, 230–240. [CrossRef]
13. Schneider, A. Monitoring land cover change in urban and peri-urban areas using dense time stacks of Landsat satel-lite data and a data mining approach. *Remote Sens. Environ.* **2012**, *124*, 689–704. [CrossRef]
14. Hu, T. Research on Multi-Layer Classification of Urban Land Cover and Structure Types Oriented to Landsat Remote Sensing Imagery. Ph.D. Thesis, Wuhan University, Wuhan, China, 2020. Available online: https://kns.cnki.net/KCMS/detail/detail.aspx?dbname=CDFDLAST2022&filename=1020967147.nh (accessed on 1 April 2020).
15. Elvidge, C.D.; Tuttle, B.T.; Sutton, P.C.; Baugh, K.E.; Howard, A.T.; Milesi, C.; Bhaduri, B.L.; Nemani, R. Global Distribution and Density of Constructed Impervious Surfaces. *Sensors* **2007**, *7*, 1962–1979. [CrossRef] [PubMed]
16. Liu, Z.; He, C.; Zhang, Q.; Huang, Q.; Yang, Y. Extracting the dynamics of urban expansion in China using DMSP-OLS nighttime light data from 1992 to 2008. *Landsc. Urban Plan.* **2012**, *106*, 62–72. [CrossRef]
17. Xu, T.; Ma, T.; Zhou, C.; Zhou, Y. Characterizing Spatio-Temporal Dynamics of Urbanization in China Using Time Series of DMSP/OLS Night Light Data. *Remote Sens.* **2014**, *6*, 7708–7731. [CrossRef]
18. Ao, Y.; Wu, B.-L.; Bai, Z.; Wang, X.-F.; Chen, Z.-X. Spatial and temporal dynamic characteristics of urban built-up areas in Guangdong-Hong Kong-Macao Greater Bay Area based on NPP-like VIIRS nighttime lighting data. *J. Earth Sci. Environ.* **2022**, *44*, 513–523. [CrossRef]
19. Zheng, Q.; Deng, J.; Jiang, R.; Wang, K.; Xue, X.; Lin, Y.; Huang, Z.; Shen, Z.; Li, J.; Shahtahmassebi, A.R. Monitoring and assessing "ghost cities" in Northeast China from the view of nighttime light remote sensing data. *Habitat Int.* **2017**, *70*, 34–42. [CrossRef]
20. Elvidge, C.D.; Imhoff, M.L.; Baugh, K.E.; Hobson, V.R.; Nelson, I.; Safran, J.; Dietz, J.B.; Tuttle, B.T. Night-time lights of the world: 1994–1995. *ISPRS J. Photogramm. Remote Sens.* **2001**, *56*, 81–99. [CrossRef]

21. Elvidge, C.D.; Baugh, K.E.; Zhizhin, M.; Hsu, F.-C. Why VIIRS data are superior to DMSP for mapping nighttime lights. *Proc. Asia-Pac. Adv. Netw.* **2013**, *35*, 62. [CrossRef]
22. Guo, W. Nocturnal Lighting Data and MODIS Data for Large-Scale Impervious Surface Mapping. Ph.D. Thesis, Wuhan University, Wuhan, China, 2015.
23. Ding, J.; Leng, Z. A geographic analysis of regional poverty. *J. Geogr.* **2018**, *73*, 232–247.
24. Gao, B.; Huang, Q.; He, C.; Ma, Q. Dynamics of Urbanization Levels in China from 1992 to 2012: Perspective from DMSP/OLS Nighttime Light Data. *Remote Sens.* **2015**, *7*, 1721–1735. [CrossRef]
25. Liu, Q.; Zham, Q.; Li, J.; Yang, C.; Liu, W. Extracting Impermeable surfaces Using Luojia-1A Nighttime Light Im-ageries in Wuhan, China. *Geomat. Inf. Sci. Wuhan Univ.* **2021**, *46*, 30–39. [CrossRef]
26. Zhang, C.; Pei, Y.; Li, J.; Qin, Q.; Yue, J. Application of Luojia1-01 Nighttime Images for Detecting the Light Changes for the 2019 Spring Festival in Western Cities, China. *Remote Sens.* **2020**, *12*, 1416. [CrossRef]
27. Li, C.; Yang, W.; Tang, Q.; Tang, X.; Lei, J.; Wu, M.; Qiu, S. Detection of Multidimensional Poverty Using Luojia1-01 Nighttime Light Imagery. *J. Indian Soc. Remote Sens.* **2020**, *48*, 963–977. [CrossRef]
28. Wang, X.; Zhou, T.; Tao, F.; Zang, F. Correlation Analysis between UBD and LST in Hefei, China, Using Luojia1-01 Night-Time Light Imagery. *Appl. Sci.* **2019**, *9*, 5224. [CrossRef]
29. Li, X.; Zhao, L.; Han, W.; Faouzi, B.; Washaya, P.; Zhang, X.; Jin, H.; Wu, C. Evaluating Algeria's social and economic development using a series of night-time light images between 1992 to 2012. *Int. J. Remote Sens.* **2018**, *39*, 9228–9248. [CrossRef]
30. Li, X.; Zhou, W. Dasymetric mapping of urban population in China based on radiance corrected DMSP-OLS nighttime light and land cover data. *Sci. Total Environ.* **2018**, *643*, 1248–1256. [CrossRef]
31. Pauwels, J.; Le Viol, I.; Azam, C.; Valet, N.; Julien, J.-F.; Bas, Y.; Lemarchand, C.; de Miguel, A.S.; Kerbiriou, C. Accounting for artificial light impact on bat activity for a biodiversity-friendly urban planning. *Landsc. Urban Plan.* **2018**, *183*, 12–25. [CrossRef]
32. Hu, W.; Liu, C.; Zhan, Q. Synthesis method and comparative verification of annual nighttime light data of npp-viirs in China. *J. Guilin Univ. Technol.* **2021**, *41*, 8.
33. Zhang, G.; Wang, J.; Jiang, Y.; Zhou, P.; Zhao, Y.; Xu, Y. On-Orbit Geometric Calibration and Validation of Luojia1-01 Night-Light Satellite. *Remote Sens.* **2019**, *11*, 264. [CrossRef]
34. Sutton, P.; Roberts, D.; Elvidge, C.; Meij, H. A Comparison of Nighttime Satellite Imagery. *Photogramm. Eng. Remote Sens.* **1997**, *63*, 1303–1313.
35. Imhoff, M.L.; Lawrence, W.T.; Stutzer, D.C.; Elvidge, C.D. A technique for using composite DMSP/OLS "city lights" sat-ellite data to map urban area. *Remote Sens. Environ.* **1997**, *61*, 361–370. [CrossRef]
36. Miller, S.D.; Mills, S.P.; Elvidge, C.D.; Lindsey, D.T.; Lee, T.F.; Hawkins, J.D. Suomi satellite brings to light a unique frontier of nighttime environmental sensing capabilities. *Proc. Natl. Acad. Sci. USA* **2012**, *109*, 15706–15711. [CrossRef] [PubMed]
37. Cao, Z.; Wu, Z.; Kuang, Y.; Huang, N. Correction and application of Dmsp/ols nighttime light imagery for the Chinese region. *J. Geoinform. Sci.* **2015**, *17*, 11.
38. Vapnik, V.; Chapelle, O. Bounds on Error Expectation for Support Vector Machines. *Neural Comput.* **2000**, *12*, 2013–2036. [CrossRef] [PubMed]
39. Mazzoni, D.; Horváth, Á.; Garay, M.J.; Tang, B.; Davies, R. A MISR Cloud-Type Classifier Using Reduced Support Vector Machines[C]//Eighth Workshop on Mining Scientific. 2005; Volume 19. Available online: https://ml.jpl.nasa.gov/papers/mazzoni/mazzoni-msd05-misr.pdf (accessed on 17 December 2022).
40. Levin, N.; Kyba, C.C.; Zhang, Q.; de Miguel, A.S.; Román, M.O.; Li, X.; Portnov, B.A.; Molthan, A.L.; Jechow, A.; Miller, S.D.; et al. Remote sensing of night lights: A review and an outlook for the future. *Remote Sens. Environ.* **2019**, *237*, 111443. [CrossRef]
41. Ma, T. An Estimate of the Pixel-Level Connection between Visible Infrared Imaging Radiometer Suite Day/Night Band (VIIRS DNB) Nighttime Lights and Land Features across China. *Remote Sens.* **2018**, *10*, 723. [CrossRef]
42. Wang, Y.; Shen, Z. Comparing Luojia1-01 and VIIRS Nighttime Light Data in Detecting Urban Spatial Structure Using a Threshold-Based Kernel Density Estimation. *Remote Sens.* **2021**, *13*, 1574. [CrossRef]
43. Guo, B.; Bian, Y.; Zhang, D.; Su, Y.; Wang, X.; Zhang, B.; Wang, Y.; Chen, Q.; Wu, Y.; Luo, P. Estimating Socio-Economic Parameters via Machine Learning Methods Using Luojia1-01 Nighttime Light Remotely Sensed Images at Multiple Scales of China in 2018. *IEEE Access* **2021**, *9*, 34352–34365. [CrossRef]
44. Li, F.; Liu, X.; Liao, S.; Jia, P. The Modified Normalized Urban Area Composite Index: A Satelliate-Derived High-Resolution Index for Extracting Urban Areas. *Remote Sens.* **2021**, *13*, 2350. [CrossRef]
45. Gong, P.; Li, X.; Wang, J.; Bai, Y.; Chen, B.; Hu, T.; Liu, X.; Xu, B.; Yang, J.; Zhang, W.; et al. Annual maps of global artificial impervious area (GAIA) between 1985 and 2018. *Remote Sens. Environ.* **2019**, *236*, 111510. [CrossRef]
46. Xu, Z.; Gao, X. A novel method for identifying the boundary of urban Impermeable surfaces with POI data. *Acta Geogr. Sin.* **2016**, *71*, 928–939.
47. Wu, S.P.; Zhou, Z.F.; Zhu, M.; Huang, D.H.; Peng, R.W. Spatial and temporal characteristics of drought in different landform types in a typical karst agglomeration. *Soil Water Conserv. Res.* **2023**, *1*, 336–347. [CrossRef]
48. Ou, J.; Liu, X.; Liu, P.; Liu, X. Evaluation of Luojia1-01 nighttime light imagery for impervious surface detection: A comparison with NPP-VIIRS nighttime light data. *Int. J. Appl. Earth Obs. Geoinf.* **2019**, *81*, 1–12. [CrossRef]

49. Tang, F.; Xu, H. Impervious Surface Information Extraction Based on Hyperspectral Remote Sensing Imagery. *Remote Sens.* **2017**, *9*, 550. [CrossRef]
50. Kotarba, A.Z.; Aleksandrowicz, S. Impervious surface detection with nighttime photography from the International Space Station. *Remote Sens. Environ.* **2016**, *176*, 295–307. [CrossRef]